

Adjusting the Potential Field Source Surface Height Based on MHD Simulations

ZHENGUANG HUANG,¹ GÁBOR TÓTH,¹ JIA HUANG,² NISHTHA SACHDEVA,¹ BART VAN DER HOLST,¹
AND WARD B. MANCHESTER¹

¹*Climate and Space Sciences and Engineering, University of Michigan, Ann Arbor, MI 48109, USA*

²*Space Sciences Laboratory, University of California, Berkeley, CA 94720, USA.*

ABSTRACT

A potential field solution is widely used to extrapolate the coronal magnetic field above the Sun's surface to a certain height. This model applies the current-free approximation and assumes that the magnetic field is entirely radial beyond the source surface height, which is defined as the radial distance from the center of the Sun. Even though the source surface is commonly specified at $2.5 R_s$ (solar radii), previous studies have suggested that this value is not optimal in all cases. In this study, we propose a novel approach to specify the source surface height, by comparing the areas of the open magnetic field regions from the potential field solution with predictions made by a magnetohydrodynamics model, in our case the Alfvén Wave Solar atmosphere Model. We find that the adjusted source surface height is significantly less than $2.5 R_s$ near solar minimum, and slightly larger than $2.5 R_s$ near solar maximum. We also report that the adjusted source surface height can provide a better open flux agreement with the observations near the solar minimum, while the comparison near the solar maximum is slightly worse.

1. INTRODUCTION

The magnetic field configuration in the solar corona is critical to understanding the physics of the solar corona as it is highly associated with the origin of the fast and slow solar wind according to several theories including the flux expansion model (Wang & Sheeley 1990; Arge & Pizzo 2000) and the separatrix–web (S-web) model (Antiochos et al. 2011; Titov et al. 2011). The coronal magnetic structure defines the structure of the entire heliosphere including the location of the helispheric current sheet (McComas et al. 2002), the distribution of ion charge state (Oran et al. 2013), and the formation and evolution of stream interaction regions (Gosling & Pizzo 1999)

There are different approaches in constructing the magnetic field in the solar corona. For example, to obtain the global coronal structures, the potential field source surface model (Altschuler & Newkirk 1969; Schatten et al. 1969) and non-force free models (Bogdan & Low 1986; Neukirch 1995; Hu & Dasgupta 2008) are applied. Besides, more sophisticated Magnetohydrodynamics (MHD) models such as the Magnetohydrodynamic Algorithm outside a Sphere (MAS, Mikić et al. (1999)), the hybrid solar wind model of Feng et al. (2011) and the Alfvén Wave Solar atmosphere Model (AW-SoM, Sokolov et al. (2013); van der Holst et al. (2014)) are also used. For active regions, linear force-free models (Alissandrakis 1981; Gary 1989), non-linear force-free models (Schrijver et al. 2006; Aschwanden & Malanushenko 2013) and non-force free models (Hu et al. 2008) are typically used.

The Potential Field Source Surface (PFSS, Altschuler & Newkirk (1969); Schatten et al. (1969)) model is the simplest model and widely used for extrapolating the magnetic field in the solar corona based on the observed photospheric magnetic field. It assumes a current-free magnetic field configuration in the solar corona. Under this assumption, the magnetic field equation can be simplified as the Laplace equation as $\nabla^2\phi = 0$, where ϕ is the scalar potential of the magnetic field. The inner boundary is usually specified by the observed photospheric magnetic field (a magnetogram); and a purely radial magnetic field is assumed at the outer boundary, which is also called the source surface and usually at $2.5 R_s$ (solar radii). The magnetic field can be obtained as $\mathbf{B} = \nabla\phi$ after solving the Laplace equation.

The simple PFSS model has very limited adjusted parameters: the height and or the shape of the source surface. For the traditional spherical shape of the source surface, [Altschuler & Newkirk \(1969\)](#) have suggested that the value is within 1.5 to 4.0 R_s . They also compared the magnetic field structures with white-light coronagraph observations and concluded that the source surface of 2.5 R_s best represented the overall structures. [Lee et al. \(2011\)](#) used the synoptic photospheric magnetic field map from the Mount Wilson Observatory (MWO) and investigated the source surface height by comparing the observed coronal holes and the interplanetary field strength as well as polarity measurements during minimum periods in the solar cycles 22 and 23, and concluded that the optimal height is between 1.5 to 1.9 R_s , which is significant less than the typically used value of 2.5 R_s . Recently, [Nikolić \(2019\)](#) derived the open solar magnetic flux and coronal holes for various heights of the PFSS model and found that source surface was significantly lower than 2.5 R_s during the active phase of solar cycle 24. [Badman et al. \(2020\)](#) explored the source surface height and suggested an extraordinarily low source surface height (1.3 - 1.5 R_s) can predict the small-scale polarity inversions observed by the first Parker Solar Probe (PSP) encounter between October 15 and November 30 in 2018. On the other hand, the non-spherical shape of the source surface was proposed in early 1980s ([Levine et al. 1982](#)). A follow-up study by [Schulz \(1997\)](#) also investigated the non-spherical source surface which was formulated with $F = r^{-k} \tilde{B}$, where r is the heliocentric distance and \tilde{B} is the scalar magnitude of the magnetic field produced by currents inside the Sun. They found that $k \approx 1.4$ was a good choice when they compared their results with MHD solutions for a single rotation between May and June 1993. More recently, [Kruse et al. \(2020\)](#) developed a numerical solver for an elliptic source surface of the PFSS model and investigated the different magnetic field configurations between the spherical and elliptical source surfaces. [Kruse et al. \(2021\)](#) mapped the in situ solar wind observations from the Advanced Composition Explorer (ACE) and Solar TERrestrial Relations Observatory (STEREO) back to the source surface with the ballistic mapping technique, and compared the predicted magnetic field polarity at the source surface. They showed that the PFSS model with oblate elliptical source surfaces elongated along the solar equatorial plane performed

slightly better than the traditional spherical shape. They also suggested that the non-spherical shape of the source surface was more important in solar minimum than in solar maximum.

The source surface height can also affect the predicted solar wind speed and density with the Wang-Sheeley-Arge (WSA) model (Wang & Sheeley 1990, 1992; Arge & Pizzo 2000), one of the widely used semi-empirical solar wind models in the community. Meadors et al. (2020) used data assimilation with particle filtering (sequential Monte Carlo) to adjust the height of the source surface and found that solar wind predictions can improve by varying the height of the source surface. On the other hand, Issan et al. (2023) argued that the source surface height does not play a critical role in changing the simulated solar wind with their Bayesian inference and global sensitivity analysis, compared to other parameters of the WSA model. However, their analysis was limited to three Carrington Rotations (CRs) during the declining phase of solar cycle 23, and it is unclear whether their conclusion is valid during the entire solar cycle.

In this study, we propose a novel approach in adjusting the source surface height by comparing the magnetic field structures from the PFSS and AWSoM models. Section 2 briefly describes the PFSS and AWSoM models. Section 3 discusses how we adjust the source surface height based on AWSoM simulation results. Finally, Section 4 draws our conclusions.

2. METHODOLOGY

The PFSS model assumes that the magnetic field is current-free in the solar corona between the solar surface and the source surface. Tóth et al. (2011) proposed two approaches to obtain the potential field solution from the Laplace equation: 1. a spherical harmonics expansion based on a uniform latitude grid; 2. a finite difference solver. We use the spherical harmonics expansion and choose the degree of spherical harmonics to be 180 in this study based on the 1 degree longitudinal resolution of the magnetogram. The spherical harmonics solution is evaluated on a uniform spherical grid with 150, 180 and 360 cells in the radial, latitudinal and longitudinal directions, respectively. The radial coordinate extends from the solar surface at $r = 1 R_s$. The source surface height is varied between 1.5 and 3.5 R_s to explore how this parameter impacts the open field area as well as the open flux, while the default source surface height is 2.5 R_s . In order to directly compare with the MHD

solutions in [Huang et al. \(2023\)](#), we use the same ADAPT-GONG magnetograms as inputs, which are listed in Table 1.

For our study, the coronal magnetic fields are provided by the AWSoM simulations, which are described in [Huang et al. \(2023\)](#). AWSoM is a first-principle based MHD model, which assumes that the nonlinear dissipation and pressure gradient from the Alfvén wave turbulence is the only source to drive the solar wind and heat the solar corona. It is implemented in the BATS-R-US (Block Adaptive Tree Solar Wind Roe-type Upwind Scheme) code ([Groth et al. 2000](#); [Powell et al. 1999](#)) within the Space Weather Modeling Framework (SWMF) ([Tóth et al. 2005, 2012](#); [Gombosi et al. 2021](#)). There is only one observational data input for the model: the observed radial component of the photospheric magnetic field at the inner boundary. At the inner boundary, a uniform density ($n=2\times 10^{17} \text{ m}^{-3}$) and temperature ($T=50,000 \text{ K}$) distribution is specified. And at the outer boundary, a zero gradient condition is applied so that the solar wind can freely leave the simulation domain. [Sokolov et al. \(2013\)](#) and [van der Holst et al. \(2014\)](#) described the physics within AWSoM in great detailed while [van der Holst et al. \(2022\)](#) discussed the recent improvement of the Alfvén wave turbulence cascade. AWSoM results have shown reasonable agreement with in-situ and remote observations under different solar wind conditions ([Jin et al. 2012](#); [Oran et al. 2013](#); [van der Holst et al. 2019](#); [Sachdeva et al. 2019](#); [Sachdeva et al. 2021](#); [Huang et al. 2023](#); [van der Holst et al. 2022](#); [Szente et al. 2022, 2023](#); [Shi et al. 2024](#)) and widely used in the community ([Jian et al. 2016](#); [Lloveras et al. 2020](#); [Henadhira Arachchige et al. 2022](#)).

3. ADJUSTING THE SOURCE SURFACE HEIGHT

We first compare the open field areas obtained from the PFSS and AWSoM models with the commonly used source surface height as $2.5 R_s$, which are shown in Figure 1. The AWSoM results are directly obtained from [Huang et al. \(2023\)](#). It can be readily noticed that the open field areas from the AWSoM simulations (in black) tend to give larger values near the solar minimum and slightly smaller values near the solar maximum, than the PFSS results (in red). The ratio between

the open field area from the MHD solution and the PFSS solution can be as large as 1.75 for CR2106 (near solar minimum) and as small as 0.8 for CR2154 (near solar maximum).

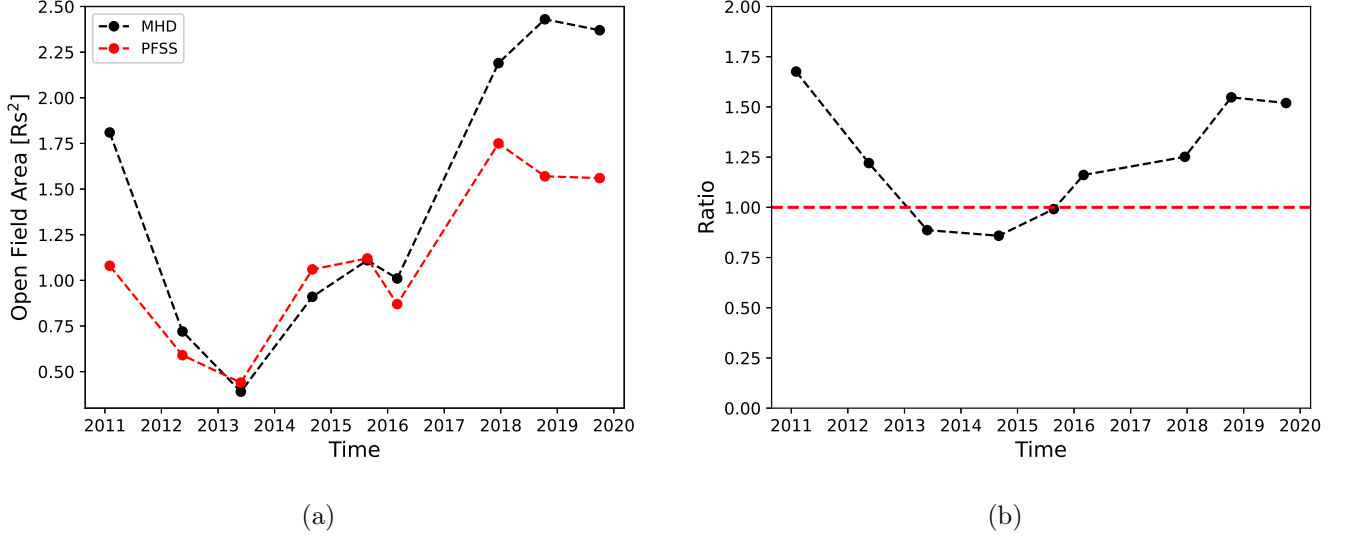


Figure 1. Panel (a) shows the open field areas obtained from the optimal AWSoM simulations (in black) and the PFSS model (in red) for all the Carrington rotations simulated in Table 1, while Panel (b) plots the ratio between the AWSoM and the PFSS open field areas. The horizontal red dashed line indicates the ratio of 1.

A natural question is, can the source surface height of the PFSS model be inferred from AWSoM simulations? To be specific, the source surface height for the PFSS model is adjusted so that it gives a similar open field area as the AWSoM results. In order to explore this idea, we obtain the PFSS solutions with different heights of the source surface, between $1.5 R_s$ and $3.5 R_s$ with the step size as $0.1 R_s$. We also derive the open and closed regions by tracing magnetic field lines on a refined grid of every 0.5 degree by 0.5 degree in both latitudinal and longitudinal directions at $1.01 R_s$ to avoid tiny closed loops. Figure 2 shows how the open field area changes with different heights of the source surface for CR2106 near solar minimum and CR2137 near solar maximum. Based on Figure 2, we conclude that the open field area monotonically increases as the source surface height decreases. And in order to obtain similar open field areas as AWSoM, the adjusted source surface heights are $1.6 R_s$ and $2.7 R_s$ for CR2106 and CR2137, respectively.

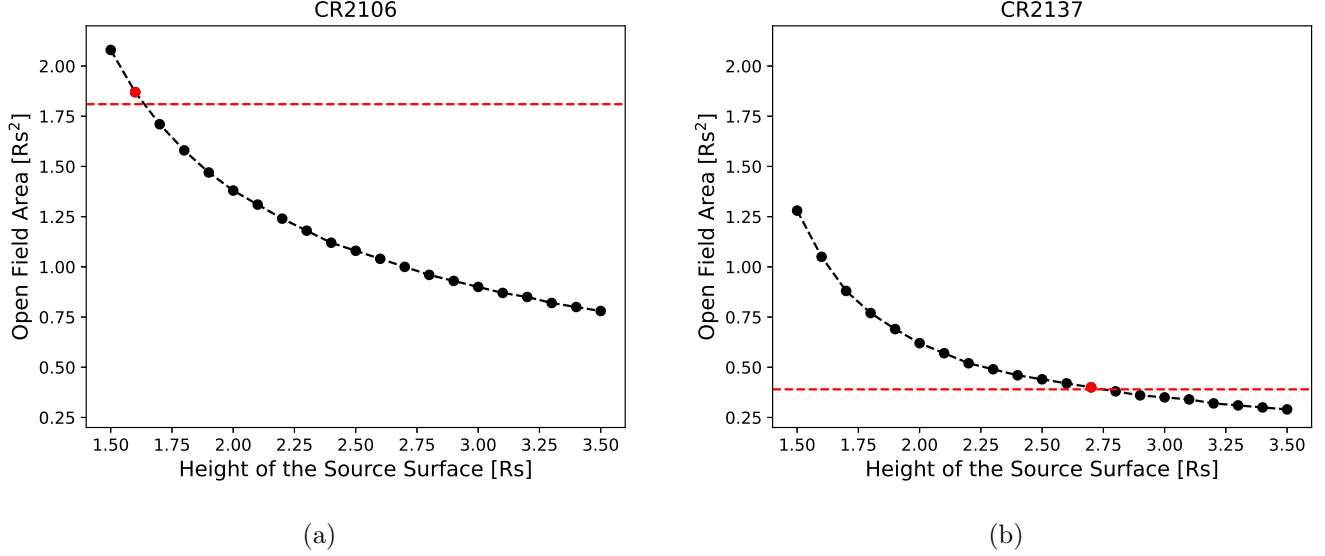


Figure 2. The open field area variations with different source surface heights for CR2106 (Panel (a)) and CR2137 (Panel(B)), respectively. The red spheres show the open field areas obtained from the adjusted source surface and the horizontal red dashed lines indicate the open field areas from the AWSoM results.

The next step is to examine the magnetic field structures between the PFSS and AWSoM results. Figure 3 shows the magnetic field configurations on the $X = 0$ plane for the PFSS model (with the default and adjusted source surface heights) and the AWSoM results. If we only consider the magnetic field structures within the PFSS domain with the default source surface height of $2.5 R_s$, then the magnetic field topology of the PFSS model is very different from the AWSoM solution for CR2106, especially in the lower right and upper left sides where the streamers form. The PFSS fieldlines are more rounded at larger height as compared to the AWSoM fieldlines. However, if the source surface height is adjusted to $1.6 R_s$, the magnetic field topology in the PFSS domain is similar to the AWSoM configuration. We conclude that the magnetic field topology of the adjusted source surface height is closer to the AWSoM result if we only consider the topology in the PFSS domain. For CR2137, as the adjusted source surface height is very close to the default height, the differences between the two PFSS solutions are not significant, and both of them are in reasonable agreement with the AWSoM result.

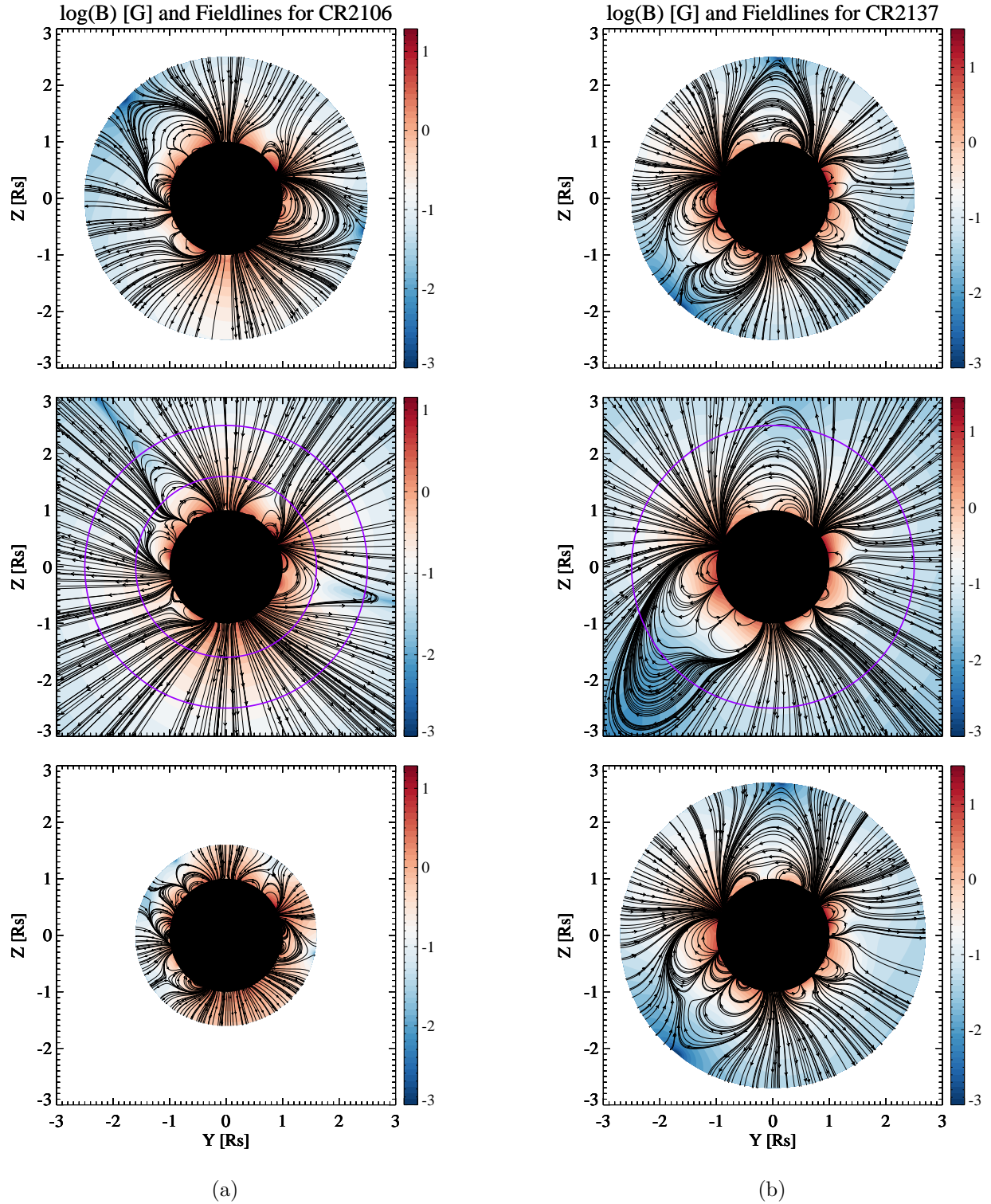


Figure 3. The magnetic field configurations from the PFSS model with the default SS height (top panels) and the adjusted source surface height (bottom panels), as well as from the AWSOM simulations (middle panels). The color bars show the magnetic field magnitude in log scale. Column (a) shows the results for CR2106 while Column (b) plots the results for CR2137, respectively. In Panel (a), the outer purple circle indicates the default source surface height of $2.5 R_s$ while the inner purple circle is associated with the adjusted source surface height of $1.6 R_s$. In Panel (b), the purple circle indicates the default source surface height of $2.5 R_s$.

Figure 4 compares the open field regions (at $1.01 R_s$) obtained from the PFSS model with the default and adjusted source surface heights as well as the AWSoM results. For CR2106 near solar minimum, we can immediately see the differences between the two source surface heights, and the open field regions obtained from the adjusted source surface height is closer to the AWSoM solution. For CR2137 near solar maximum, the differences between the two source surface heights are not significant and can hardly be distinguished visibly; and fortunately, both PFSS model results are similar to the AWSoM results.

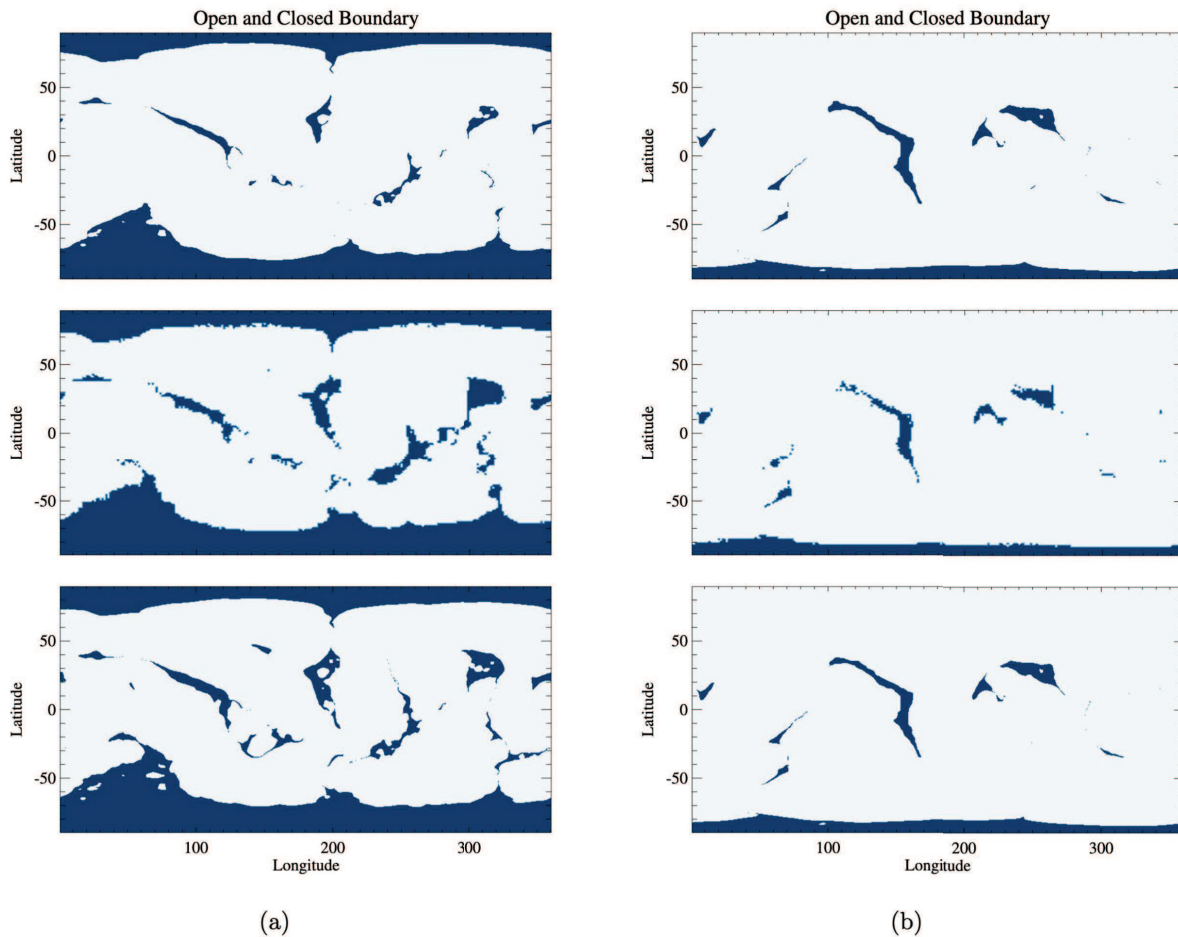


Figure 4. The blue areas show the open field regions from the PFSS model with the default SS height (top panels) and the adjusted SS height (bottom panels), as well as from the AWSoM simulation (middle panels). Column (a) shows the results for CR2106 while Column (b) plots the results for CR2137, respectively.

CR	UTC Time of Map	Adjusted Source Surface Height [R_s]	Open Flux [Gauss R_s^2]			
			AWSOM	Default PFSS	Adjusted PFSS	Observed
2106	2011-2-2 02:00:00	1.6	9.39	4.83	9.67	13.76
2123	2012-5-16 20:00:00	2.2	7.99	5.15	6.45	13.84
2137	2013-5-28 20:00:00	2.7	5.88	5.88	5.32	13.74
2154	2014-9-2 20:00:00	2.7	10.07	9.61	8.47	16.17
2167	2015-8-23 02:00:00	2.5	15.18	13.36	13.36	17.37
2174	2016-3-3 02:00:00	2.3	11.13	8.51	9.6	14.71
2198	2017-12-17 02:00:00	1.9	11.45	8.31	10.58	15.22
2209	2018-10-13 06:00:00	1.7	12.32	7.88	10.89	12.12
2222	2019-10-2 02:00:00	1.7	11.85	7.93	10.55	14.41

Table 1. The adjusted source surface heights and open fluxes for all the ADAPT-GONG magnetograms.

We carry out the same analysis for other CRs in [Huang et al. \(2023\)](#) and the results are summarized in [Table 1](#). The adjusted source surface height is below $2.0 R_s$ near solar minimum conditions while it is slightly above $2.5 R_s$ near solar maximum conditions. In addition, we calculate the open flux, which is the integral of the unsigned radial component of the magnetic field (B_r) in the open field regions. [Table 1](#) shows that the open flux increases as the source surface height is reduced. Moreover, we calculate the open flux from Wind observations at 1 AU based on the equation $4\pi R_{1AU}^2 |B_{r,1AU}|$ (e.g. [Wang et al. 2000](#); [Linker et al. 2017](#)), where $R_{1AU} = 215 R_s$ and $|B_{r,1AU}|$ is the absolute value of the radial magnetic field strength at 1 AU. The open fluxes from the PFSS model with adjusted source surface heights are closer to AWSOM results and the observations, except for CR2137 and CR2154 near solar maximum.

4. SUMMARY AND DISCUSSIONS

We propose a novel approach to adjust the source surface height of the PFSS model by matching the size of the open field area to an MHD model, e.g., AWSOM. The PFSS model is widely used in the community to study the magnetic field structures of the solar corona. The source surface height is regularly set at $2.5 R_s$. On the other hand, there are studies arguing this “default” value may not be the optimal value ([Lee et al. 2011](#); [Nikolić 2019](#); [Badman et al. 2020](#)). The magnetic field structures obtained from an MHD model are considered to be more accurate than the PFSS model,

as the MHD model does not employ specific assumptions (i.e., current-free and radial field beyond the source surface) to extrapolate the magnetic field from the observed photospheric magnetic field. Our new approach connects the magnetic field topology from the PFSS and AWSoM results. Our results suggest that the source surface height is smaller than the default height of $2.5 R_s$ during solar minimum, while it is slightly larger than the $2.5 R_s$ during solar maximum. We also find that the PFSS model with the adjusted source surface height can give similar open field regions as the AWSoM results provided in [Huang et al. \(2023\)](#).

We compare the magnetic field structures on $X = 0$ plane from the AWSoM simulations and the PFSS solutions with different source surface heights. We notice that the magnetic field structures from the adjusted source surface height are closer to the AWSoM configurations, if we only consider the topology within the PFSS domain, especially during solar minimum. In the solar minimum conditions, there are very few active regions. Due to the solar wind acceleration, the magnetic fields are dragged in the radial direction, as seen in the helmet streamers in the middle panels in [Figure 3](#), which may explain the reduced source surface height. In the solar maximum conditions, there are very strong active regions, which bring large coronal loops over those regions. In this case, the source surface height needs to increase to capture the large coronal loops over the active regions. We further determine that the Spearman's correlation coefficient between the adjusted source surface height ($r_{adjusted}$) and the average unsigned B_r in the closed field regions (at $1.01 R_s$ where we determine the open and closed regions from the PFSS solution with the source surface height of $2.5 R_s$) is 0.84. Using the linear regression method, we then find that they can be empirically formulated as:

$$r_{adjusted} = 0.14 \cdot |B_r| + 1.38 \pm 0.17 \quad (1)$$

where the average unsigned B_r is in the unit of Gauss and $r_{adjusted}$ is in the unit of solar radii. [Figure 5](#) shows the linear regression results.

The discrepancy between the open flux from observations and models is one of the unsolved problems in the community ([Linker et al. 2017](#)). [Lee et al. \(2011\)](#) have explored varying the source surface heights to match the observed open flux. But their approach was limited to comparing the PFSS

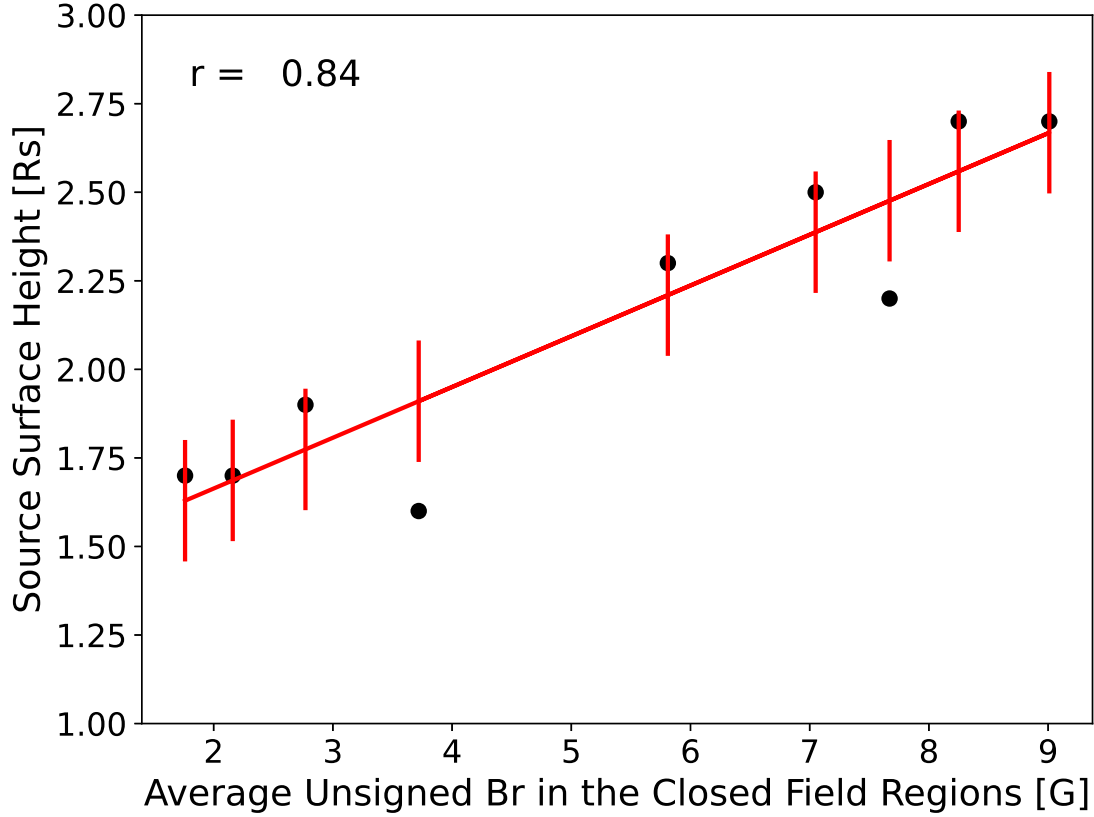


Figure 5. The black circles plot the adjusted source surface heights along with the average unsigned B_r in the closed field regions and the red line shows the linear regression between them, where the error bars show the standard deviation of the linear regression. The Spearman's correlation is shown in the upper left corner.

results with various observations. Our approach is different as we try to connect the magnetic field structures between the PFSS and AWSoM. The proposed adjusted source surface height gives larger open fluxes during the solar minimum conditions, which are closer to the observed open fluxes. Near solar maximum, the PFSS model with adjusted source surface height gives less open flux, which makes the comparison with the observations worse. Based on Figure 3, we notice large coronal loops over strong magnetic field regions, which may bring significant open fluxes originated from active regions residing near the open and closed boundaries as suggested by [Arge et al. \(2023\)](#).

Last but not least, our work is limited to the spherical shape of the source surface for the PFSS model. Recent work has suggested that a non-spherical shape of the source surface is important during solar minimum and less important during solar maximum (Kruse et al. 2021) . It is important to investigate how the non-spherical shape evolves during a solar rotation. However, this is beyond the scope of the manuscript as our study focuses on how to adjust the height of spherical source surface based on MHD solutions. More work is needed in this direction in the future.

This work was primarily supported by the NSF PRE-EVENTS grant No. 1663800, the NSF SWQU grant No. PHY-2027555, the NSF Solar Terrestrial grant No. 2323303, and the NASA grants Nos. 80NSSC22K0892, 80NSSC22K0269 and 80NSSC23K0450. J. Huang is also supported by the NASA grant 80NSSC23K0737.

We acknowledge the high-performance computing support from Cheyenne (doi:10.5065/D6RX99HX) provided by NCAR’s Computational and Information Systems Laboratory, sponsored by the NSF, and the computation time on Frontera (doi:10.1145/3311790.3396656) sponsored by NSF and the NASA supercomputing system Pleiades.

This work utilizes data produced collaboratively between AFRL/ADAPT and NSO/NISP.

REFERENCES

- Alissandrakis, C. E. 1981, *A&A*, 100, 197
- Altschuler, M. D., & Newkirk, G. 1969, *SoPh*, 9, 131
- Antiochos, S. K., Mikić, Z., Titov, V. S., Lionello, R., & Linker, J. A. 2011, *ApJ*, 731, 112
- Arge, C. N., Leisner, A., Wallace, S., & Henney, C. J. 2023, arXiv e-prints, arXiv:2304.07649
- Arge, C. N., & Pizzo, V. J. 2000, *J. Geophys. Res.*, 105, 10465
- Aschwanden, M. J., & Malanushenko, A. 2013, *SoPh*, 287, 345
- Badman, S. T., Bale, S. D., Martínez Oliveros, J. C., et al. 2020, *ApJS*, 246, 23
- Bogdan, T. J., & Low, B. C. 1986, *ApJ*, 306, 271
- Feng, X., Zhang, S., Xiang, C., et al. 2011, *ApJ*, 734, 50
- Gary, G. A. 1989, *ApJS*, 69, 323
- Gombosi, T. I., Chen, Y., Glocer, A., et al. 2021, *Journal of Space Weather and Space Climate*, 11, 42
- Gosling, J. T., & Pizzo, V. J. 1999, *SSRv*, 89, 21

- Groth, C. P. T., De Zeeuw, D. L., Gombosi, T. I., & Powell, K. G. 2000, *J. Geophys. Res.*, 105, 25053
- Henadhira Arachchige, K., Cohen, O., Munoz-Jaramillo, A., & Yeates, A. R. 2022, *ApJ*, 938, 39
- Hu, Q., & Dasgupta, B. 2008, *SoPh*, 247, 87
- Hu, Q., Dasgupta, B., Choudhary, D. P., & Büchner, J. 2008, *ApJ*, 679, 848
- Huang, Z., Tóth, G., Sachdeva, N., et al. 2023, *ApJL*, 946, L47
- Issan, O., Riley, P., Camporeale, E., & Kramer, B. 2023, *Space Weather*, 21, e2023SW003555
- Jian, L. K., MacNeice, P. J., Mays, M. L., et al. 2016, *Space Weather*, 14, 592
- Jin, M., Manchester, W. B., van der Holst, B., et al. 2012, *ApJ*, 745, 6
- Kruse, M., Heidrich-Meisner, V., & Wimmer-Schweingruber, R. F. 2021, *A&A*, 645, A83
- Kruse, M., Heidrich-Meisner, V., Wimmer-Schweingruber, R. F., & Hauptmann, M. 2020, *A&A*, 638, A109
- Lee, C. O., Luhmann, J. G., Hoeksema, J. T., et al. 2011, *SoPh*, 269, 367
- Levine, R. H., Schulz, M., & Frazier, E. N. 1982, *SoPh*, 77, 363
- Linker, J., Caplan, R., Downs, C., et al. 2017, *The Astrophysical Journal*, 848, 70
- Lloveras, D. G., Vázquez, A. M., Nuevo, F. A., et al. 2020, *SoPh*, 295, 76
- McComas, D. J., Elliott, H. A., Gosling, J. T., et al. 2002, *Geophys. Res. Lett.*, 29, 1290
- Meadors, G. D., Jones, S. I., Hickmann, K. S., et al. 2020, *Space Weather*, 18, e02464
- Mikić, Z., Linker, J. A., Schnack, D. D., Lionello, R., & Tarditi, A. 1999, *Physics of Plasmas*, 6, 2217
- Neukirch, T. 1995, *A&A*, 301, 628
- Nikolić, L. 2019, *Space Weather*, 17, 1293
- Oran, R., van der Holst, B., Landi, E., et al. 2013, *ApJ*, 778, 176
- Powell, K. G., Roe, P. L., Linde, T. J., Gombosi, T. I., & de Zeeuw, D. L. 1999, *Journal of Computational Physics*, 154, 284
- Sachdeva, N., van der Holst, B., Manchester, W. B., et al. 2019, *ApJ*, 887, 83
- Sachdeva, N., Tóth, G., Manchester, W. B., et al. 2021, *Earth and Space Science Open Archive*, 13
- Schatten, K. H., Wilcox, J. M., & Ness, N. F. 1969, *SoPh*, 6, 442
- Schrijver, C. J., De Rosa, M. L., Metcalf, T. R., et al. 2006, *SoPh*, 235, 161
- Schulz, M. 1997, *Annales Geophysicae*, 15, 1379
- Shi, T., Manchester, W., Landi, E., et al. 2024, *ApJ*, 961, 60
- Sokolov, I. V., van der Holst, B., Oran, R., et al. 2013, *ApJ*, 764, 23
- Szente, J., Landi, E., & van der Holst, B. 2022, *ApJ*, 926, 35
- . 2023, *ApJS*, 269, 37

- Titov, V. S., Mikić, Z., Linker, J. A., Lionello, R., & Antiochos, S. K. 2011, *ApJ*, 731, 111
- Tóth, G., van der Holst, B., & Huang, Z. 2011, *ApJ*, 732, 102
- Tóth, G., Sokolov, I. V., Gombosi, T. I., et al. 2005, *Journal of Geophysical Research (Space Physics)*, 110, 12226
- Tóth, G., van der Holst, B., Sokolov, I. V., et al. 2012, *Journal of Computational Physics*, 231, 870
- van der Holst, B., Manchester, W. B., I., Klein, K. G., & Kasper, J. C. 2019, *ApJL*, 872, L18
- van der Holst, B., Sokolov, I. V., Meng, X., et al. 2014, *ApJ*, 782, 81
- van der Holst, B., Huang, J., Sachdeva, N., et al. 2022, *ApJ*, 925, 146
- Wang, Y.-M., Lean, J., & Sheeley Jr, N. 2000, *Geophysical Research Letters*, 27, 505
- Wang, Y. M., & Sheeley, N. R., J. 1990, *ApJ*, 355, 726
- . 1992, *ApJ*, 392, 310